# Structure-Based Approach for Binding Site Identification on AmpC β-Lactamase

Rachel A. Powers and Brian K. Shoichet*

*Department of Molecular Pharmacology and Biological Chemistry, Northwestern University, 303 East Chicago Avenue, Chicago, Illinois 60611*

β-Lactamases are the most widespread resistance mechanism to β-lactam antibiotics and are an increasing menace to public health. Several β-lactamase structures have been determined, making this enzyme an attractive target for structure-based drug design. To facilitate inhibitor design for the class C β-lactamase AmpC, binding site "hot spots" on the enzyme were identified using experimental and computational approaches. Experimentally, X-ray crystal structures of AmpC in complexes with four boronic acid inhibitors and a higher resolution (1.72 Å) native apo structure were determined. Along with previously determined structures of AmpC in complexes with five other boronic acid inhibitors and four β-lactams, consensus binding sites were identified. Computationally, the programs GRID, MCSS, and X-SITE were used to predict potential binding site hot spots on AmpC. Several consensus binding sites were identified from the crystal structures. An amide recognition site was identified by the interaction between the carbonyl oxygen in the R1 side chain of β-lactams and the atom Nδ2 of the conserved Asn152. Surprisingly, this site also recognizes the aryl rings of arylboronic acids, appearing to form quadrupole−dipole interactions with Asn152. The highly conserved "oxyanion" hole defines a site that recognizes both carbonyl and hydroxyl groups. A hydroxyl binding site was identified by the O2 hydroxyl in the boronic acids, which hydrogen bonds with Tyr150 and a conserved water. A hydrophobic site is formed by Leu119 and Leu293. A carboxylate binding site was identified by the ubiquitous C3(4) carboxylate of the β-lactams, which interacts with Asn346 and Arg349. Four water sites were identified by ordered waters observed in most of the structures; these waters form extensive hydrogen-bonding networks with AmpC and occasionally the ligand. Predictions by the computational programs showed some correlation with the experimentally observed binding sites. Several sites were not predicted, but novel binding sites were suggested. Taken together, a map of binding site hot spots found on AmpC, along with information on the functionality recognized at each site, was constructed. This map may be useful for structure-based inhibitor design against AmpC.

## Introduction

β-Lactamases are the most widespread resistance mechanism to β-lactam antibiotics, hydrolyzing and inactivating penicillins, cephalosporins, and related molecules. Class C β-lactamases, such as AmpC, are among the most problematic of these enzymes. Not only are they widely expressed among nosocomial pathogens but also class C β-lactamases are not significantly inhibited by clinically used β-lactamase inhibitors, such as clavulanate. Moreover, they naturally have a broad spectrum of action and can hydrolyze "β-lactamase resistant" β-lactams, such as the third-generation cephalosporins. Indeed, β-lactam-based inhibitors and β-lactamase resistant β-lactams can upregulate the expression of class C β-lactamases, thereby defeating themselves.[1−3] There is a pressing need for novel, non-β-lactam-based inhibitors of these enzymes.

Since the X-ray crystal structures of class C β-lactamases were first determined,[4−7] these enzymes have been attractive targets for novel inhibitor discovery using structure-based methods. There are well-defined pockets in the binding sites that look as though they might accommodate inhibitor functionality, and extensive structure−function studies suggest a role for many of these sites.[8−11] The structures also present challenges that are typical of many enzyme targets. The active sites of these enzymes are much larger than their substrates, and some of the observed sites, however well-defined structurally, have no known function (Figure 1). Water molecules are observed to bind in some of these sites, and it is unclear whether they should be treated as displaceable or structurally integral components of the protein.[12,13]

The challenge of finding the "hot spots" for ligand binding is common to most structure-based efforts. Several techniques have been introduced to address this problem. Binding sites may be explored experimentally by using ligand molecules as probes. This can be done crystallographically, using solvent[14] or even larger molecules,[15] or by nuclear magmetic resonance (NMR), using small molecule fragments that can probe the ability of a particular site to bind to a particular functionality or group of functionalities.[16] Computational approaches are also used to identify hot spots for ligand binding. Computer programs such as GRID[17] and MCSS[18] use functional groups to probe the energy potential of protein binding sites and identify favorable

* To whom correspondence should be addressed. Tel.: 312-503-0081. Fax: 312-503-5349. E-mail: b-shoichet@northwestern.edu.
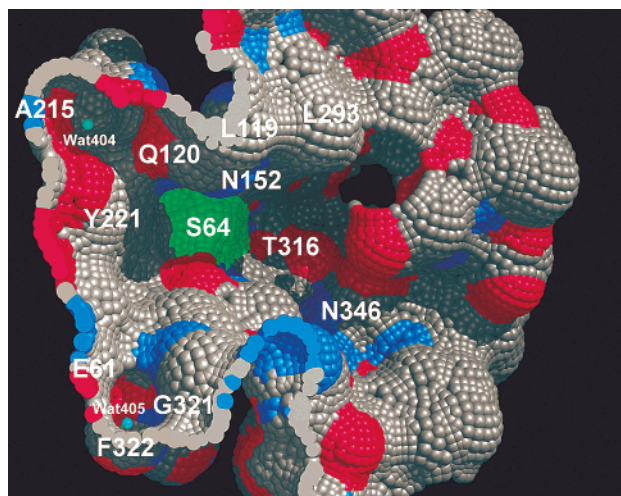
**Figure 1.** Molecular surface[58] of the active site region of AmpC. The catalytic residue Ser64 is colored green. Several conserved residues are labeled. Interesting features of AmpC that appear to be preorganized to bind a ligand are shown. A tunnel begins behind the catalytic Ser64 and extends for approximately 15 Å through the interior of AmpC and two pockets observed structurally that bind waters. The surface contributed by nitrogen atoms is colored blue, oxygen atoms are colored red, and carbon atoms are colored gray. Cyan spheres represent ordered water molecules. All figures were generated with MidasPlus,[59] unless otherwise noted.

positions for different ligand functionalities. Programs such as X-SITE[19] use knowledge-based potentials to find favorable positions for similar probe groups.

Structure-based inhibitor discovery in class C $\beta$-lactamases has proceeded without much formal effort to map the binding site for hot spots but has instead relied more on substrate and substrate−analogue approaches to lead discovery. Thus, the structure of AmpC has been determined in complex with inhibitors such as $\beta$-lactams,[4,20−22] transition state analogues,[23,24] and arylboronic acids,[6,25,26] the leads for which were known before the first structures were determined.[27] There are now 18 inhibitor complex structures with class C $\beta$-lactamases that have been published. This wealth of structural information allows us to consider a consensus view of where the hot spots for ligand binding are on class C $\beta$-lactamases and what sort of ligand groups they recognize.

Here, we use nine previously determined X-ray crystal structures to partly construct a consensus map of hot spots for functional group binding on AmpC $\beta$-lactamase (compounds **5−13**, Table 1). To further enrich the functionality explored, we determined the structures of four new inhibitor complexes by X-ray crystallography (compounds **1−4**, Tables 1−3). As a reference, we have also determined the structure of native apo AmpC to higher resolution (1.72 Å) and with better crystallographic statistics (Table 2) than was previously determined (Protein Data Bank (PDB) entry 2BLS; 2.00 Å). Functionalities displayed on these nine boronic acids and four $\beta$-lactams act as probes of the AmpC site. By overlaying these 13 experimental structures, we ask whether hot spots emerge that were not apparent when considering the individual structures separately. We also use the GRID, MCSS, and X-SITE computer programs to further probe AmpC for functional group binding sites. This allows us to investigate regions that

**Table 1.** Ligands Used to Probe the Active Site of AmpC

| Compound | Ligand | Resolution of crystal structure (Å) | R-factor/$R_{free}$ | PDB ID | $K_i$ (μM) |
|---|---|---|---|---|---|
| **1** | | 2.15 | 17.4/21.1 | 1KDS[a] | 1.7[b] |
| **2** | | 2.28 | 18.6/23.4 | 1KDW[a] | 2.9[b] |
| **3** | | 2.30 | 19.9/24.5 | 1KE0[a] | 4.2[b] |
| **4** | | 2.15 | 19.3/23.7 | 1KE3[a] | 0.20[b] |
| **5** | | 2.25 | 16.7/22.4 | 1C3B[25] | 0.027[b] |
| **6** | | 2.10 | 20.6/24.9 | 1GA9[26] | 0.08 |
| **7** | | 1.90 | 19.4/22.7 | 1FSW[24] | 0.32 |
| **8** | | 1.75 | 19.6/21.8 | 1FSY[24] | 0.150 |
| **9** | | 2.30 | 18.2/22.8 | 1IEM[33] | 0.020[c] |
| **10** loracarbef | | 2.35 | 20.8/25.7 | 1FCN[20] | NA[d] |
| **11** ceftazidime | | 2.00 | 18.2/22.6 | 1IEL[33] | NA |
| **12** cloxacillin | | 2.46 | 20.7/26.5 | 1FCM[20] | NA |
| **13** moxalactam | | 2.20 | 21.5/25.8 | 1FCO[20] | NA |
| | | 1.83 | 16.8/20.6 | 1I5Q[22] | NA |

[a] This work. [b] $K_i$ values were reported in Weston et al., 1998. [c] $K_i$ values were reported in Caselli et al., 2001. [d] NA, not applicable.

are not explored in the crystal structures and compare the computational predictions with the experimentally determined complexes.

## Results

**X-ray Crystallographic Structure Determination.** The crystal structures of AmpC in complexes with four different arylboronic acid inhibitors were determined for this study (compounds **1−4**; Tables 1−2, Figure 2A−D). The resolution of these complexes ranged from 2.15 to 2.30 Å. In each complex, the location of the inhibitor was unambiguously identified in the initial Fo−Fc difference maps when contoured at a level of 3 $\sigma$. Simulated annealing omit maps of the refined models agree well with the conformation of the inhibitors in the active sites (not shown). The quality of each of the models was analyzed with the program Procheck.[28] For the AmpC/**1** complex, 91.5% of the nonproline, nongly-

**Table 2.** Data Collection and Refinement Statistics

| | AmpC/**1** | AmpC/**2** | AmpC/**3** | AmpC/**4** | native apo AmpC |
|---|---|---|---|---|---|
| cell constants (Å; deg) | $a = 119.11$, | $a = 118.55$, | $a = 118.62$, | $a = 117.80$, | $a = 118.49$, |
| | $b = 77.73$, | $b = 77.38$, | $b = 77.43$, | $b = 78.36$, | $b = 76.97$, |
| | $c = 99.01$; | $c = 97.33$; | $c = 97.37$; | $c = 97.38$; | $c = 97.67$; |
| | $\beta = 115.86$ | $\beta = 115.30$ | $\beta = 115.32$ | $\beta = 115.93$ | $\beta = 115.90$ |
| resolution (Å) | 2.15 (2.25−2.15)[a] | 2.28 (2.37−2.28) | 2.30 (2.35−2.30) | 2.15 (2.21−2.15) | 1.72 (1.76−1.72) |
| total observations | 112 903 | 90 630 | 63 591 | 115 882 | 322 742 |
| unique observations | 43 507 | 33 450 | 33 436 | 42 306 | 81 989 |
| $R_{merge}$ (%) | 7.6 (22.2) | 7.5 (19.0) | 7.5 (23.8) | 7.5 (33.2) | 5.7 (37.2) |
| completeness (%)[b] | 98.0 (94.7) | 91.0 (62.6) | 94.2 (96.6) | 97.7 (96.3) | 98.2 (97.8) |
| $\langle I \rangle / \langle \sigma_I \times 92 \rangle$ | 9.3 (3.3) | 16.2 (3.5) | 12.2 (3.9) | 15.2 (3.7) | 23.2 (5.1) |
| resolution range for refinement (Å) | 10−2.15 | 20−2.28 | 20−2.30 | 20−2.15 | 20−1.72 |
| no. of protein residues | 716 | 716 | 716 | 716 | 710 |
| no. of water molecules | 140 | 263 | 139 | 307 | 377 |
| RMSD bond lengths (Å) | 0.008 | 0.010 | 0.010 | 0.010 | 0.012 |
| RMSD bond angles (deg) | 1.5 | 1.5 | 1.6 | 1.6 | 1.7 |
| $R$ factor (%) | 17.4 | 18.6 | 19.9 | 19.3 | 19.0 |
| $R_{free}$ (%)[c] | 21.1 | 23.4 | 24.5 | 23.7 | 21.4 |
| average $B$ factor, protein atoms (Å²) | 22.1 | 28.1 | 25.9 | 30.0 | 27.7 |
| average $B$ factor, inhibitor (Å²) | 23.3 | 30.5 | 35.7 | 33.6 | NA[d] |

[a] Values in parentheses are for the highest resolution shell. [b] Fraction of theoretically possible reflections observed. [c] $R_{free}$ was calculated with 10% of reflections set aside randomly, except for native AmpC where 5% was used. [d] Not applicable.

**Table 3.** Interactions in Complexed and Native apo AmpC $\beta$-Lactamase

| | distance (Å) | | | | | |
|---|---|---|---|---|---|---|
| | | | | | native apo AmpC | |
| interaction | AmpC/**1**[a] | AmpC/**2**[b] | AmpC/**3**[b] | AmpC/**4**[b] | molecule 1 | molecule 2 |
| S64N-O1[c] | 3.0 | 2.8 | 3.0 | 2.8 | 3.6[d] | 3.5[d] |
| A318N-O1 | 2.8 | 2.7 | 2.7 | 2.7 | 2.8[d] | 3.0[d] |
| A318N-O1 | 2.8 | 2.8 | 2.9 | 2.8 | 3.3[d] | 3.2[d] |
| Y150OH-O2[c] | 2.8 | 2.8 | 2.9 | 2.6 | NPe | NP |
| Wat402-O2 | 3.0 | 2.6 | 2.6 | 2.6 | NP | NP |
| Y150OH-K315N$\zeta$ | 2.9 | 2.9 | 2.9 | 2.9 | 2.8 | 2.8 |
| Y150OH-S64O$\gamma$ | 3.0 | 2.7 | 2.9 | 2.8 | 3.0 | 2.9 |
| Y150OH-K67N$\zeta$ | 3.5 | 3.6 | 3.5 | 3.5 | 3.4 | 3.3 |
| K67N$\zeta$-A220O | 3.0 | 2.8 | 2.9 | 2.8 | 3.0 | 2.9 |
| K67N$\zeta$-S64O$\gamma$ | 2.6 | 2.6 | 2.7 | 2.6 | 2.9 | 2.8 |
| Wat402-T316O$\gamma$1 | 3.0 | 3.0 | 3.1 | 3.0 | 3.3f | 3.0 |
| Wat402-Wat403 | 2.8 | 2.9 | 2.6 | 2.6 | 2.5[f] | 2.9 |
| Wat403-N346O$\delta$1 | 2.9 | 2.8 | 2.9 | 2.7 | 2.7[f] | 2.6 |
| Wat403-R349N$\eta$1 | 3.3 | 3.3 | 3.1 | 3.1 | 2.9[f] | 2.9 |
| N152O$\delta$1-K67N$\zeta$ | 2.6 | 2.7 | 2.7 | 2.7 | 2.6 | 2.6 |
| N152N$\delta$2-Q120O$\epsilon$1 | 6.2 | 7.3 | 7.2 | 7.1 | 7.2 | 2.8 |
| N15N$\delta$2-centroid aryl ring | 3.6 | 3.7 | 3.7 | 3.6 | NP | NP |
| centroid Y221-nearest carbon of inhibitor aryl ring | 5.0 | 4.4 | 4.2 | 4.2 | NP | NP |

[a] Distances are for molecule 2 of the asymmetric unit. [b] Distances are for molecule 1 of the asymmetric unit. [c] Atoms O1 and O2 refer to the boronic acid hydroxyls. [d] In the native structure, atom O3 of a phosphate ion (molecule 1) and Wat768 (molecule 2) are in equivalent positions to the O1 hydroxyl of the inhibitors. The distances reported here are to these analogous atoms. [e] Not present. [f] In molecule 1 of the native structure, Wat402 is displaced by O4 of the phosphate ion, and Wat403 is numbered Wat401. Distances to these atoms are reported here.

cine residues are in the most favored region of the Ramachandran plot (8.5% in the additionally allowed region); for AmpC/**2**, 91.0% of the nonproline, nonglycine residues are in the most favored region (9.0% in the additionally allowed region); for AmpC/**3**, 89.5% of the nonproline, nonglycine residues are in the most favored region (10.5% in the additionally allowed region); and for AmpC/**4**, 92.0% of the nonproline, nonglycine residues are in the most favored region (8.0% in the additionally allowed region). The structures have been deposited with the PDB as 1KDS, 1KDW, 1KE0, and 1KE3 (complexes of AmpC with **1**−**4**, respectively).

The unique portions of the inhibitors make relatively few interactions with the protein. The nitro group of **1** does not make any interactions with AmpC. The carboxylate group of **2** is 3.3 Å from N$\epsilon$2 of Gln120 in molecule 1 of the asymmetric unit, slightly long for a hydrogen bond. However, in molecule 2, this distance is 2.9 Å due to the different conformation of Gln120. The carboxylate group found in **3** interacts with a single water molecule in the site. In contrast, the structure of AmpC/**4** shows that specific polar interactions can be observed between the inhibitor and the enzyme. One hydroxyl of the terminal boronic acid group interacts with atom N$\epsilon$2 of Gln120 and atom O$\delta$1 of Asp123 (2.5 and 2.9 Å, respectively).

To provide a reference for our comparisons, the native apo structure of AmpC was determined to 1.72 Å resolution, and the coordinates and structure factors have been deposited with the PDB as 1KE4 (Tables 2−3, Figure 2E). This is a higher resolution structure than the apo structure previously determined (PDB entry 2BLS), with better crystallographic statistics, allowing for more reliable placement of side chains and water molecules. The quality of the final model was analyzed with Procheck.[28] For the nonproline, nonglycine resi-
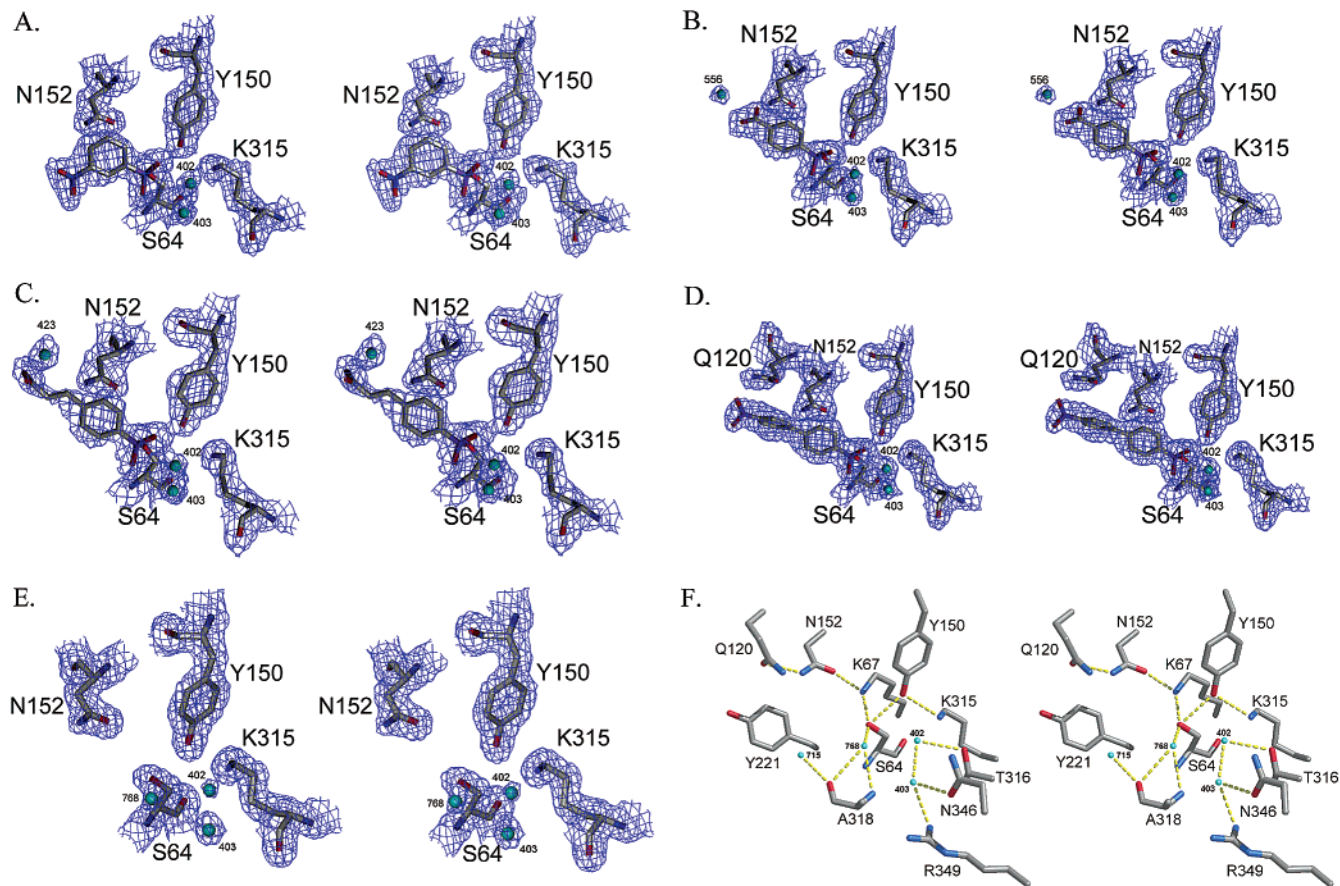
**Figure 2.** Stereoview of the active site region of both apo and complexed AmpC, focusing on representative electron density. 2Fo-Fc electron density maps are shown in blue, contoured at 1.0 $\sigma$, except for D and E, which are contoured at 0.9 $\sigma$. (A) AmpC/**1** complex; (B) AmpC/**2** complex; (C) AmpC/**3** complex; (D) AmpC/**4** complex; (E) the apo structure, determined to 1.72 Å; and (F) interactions observed in the apo active site. Dashed yellow lines indicate hydrogen bonds. Carbon atoms are colored gray, nitrogens are colored blue, and oxygens are colored red. Water molecules are represented with cyan spheres. Figure 3A−E was made with SETOR.[60]

dues, 91.8% are in the most favored region of the Ramachandran plot (8.2% in the additionally allowed region).

Overall, the higher resolution structure (1KE4) resembles the lower resolution structure (2BLS). The RMSD in all Cα atom positions of molecule 2 from each structure is 0.29 Å (for molecule 1, 0.70 Å). The RMSD in all atoms of active site residues (Ser64, Lys67, Tyr150, Asn152, and Lys315) between the two structures is 1.37 Å for molecule 1 and 1.41 Å for molecule 2. Some significant differences were observed. For instance, in the higher resolution structure, a phosphate ion was bound near Ser64 of molecule 1 (Table 3), and many more water molecules were identified (377 vs 83). The observation of an ordered phosphate ion in the active site is consistent with observations by Pratt and colleagues that class C $\beta$-lactamases are inhibited by phosphate ions at millimolar concentrations.[29] The presumed deacylating water, Wat402, was observed only in molecule 2 of 2BLS, and Wat403, a well-ordered water in the active site that hydrogen bonds with Wat402, was not observed in either molecule of the 2BLS structure. In the higher resolution structure, the completely conserved Gln120 adopts a different conformation in each molecule. In molecule 1, Gln120 is flipped out of the active site and interacts with residues Ala4 and Asn9 of a symmetry mate (Gln120Oε1−

Asn9Nδ2 = 2.8 Å; Gln120Nε2−Ala4O = 3.1 Å). In molecule 2, Gln120 points into the active site and interacts with Asn152, as observed in the 2BLS structure (Table 3, Figure 2F). Residues 285−290 of molecule 1 were excluded from the final model of the higher resolution structure, due to poor electron density.

**Consensus Binding Sites.** Along with these newly determined structures, the previously published structures of AmpC in complexes with five other boronic acids and four $\beta$-lactams were used to identify consensus binding sites (compounds **5−13**, Table 1). Individually, the structures provided little information about binding hot spots on AmpC. However, when all 13 complexes were superimposed, clear patterns emerged. Several consensus binding sites were identified in this way: an amide site, a carbonyl/hydroxyl site, a hydroxyl site, a hydrophobic site, an aryl group site, a carboxylate site, and several conserved water sites (Figure 3). Additionally, the computer programs GRID, MCSS, and X-SITE were used to identify binding sites on AmpC. We were interested to know how their predictions corresponded to the experimentally determined binding sites and also to learn of new binding sites identified by the programs but not seen crystallographically.

**Amide Binding Site.** An amide recognition site on AmpC was identified based on superposition of the complexes with **7−13** (Figure 3A). The amide groups of
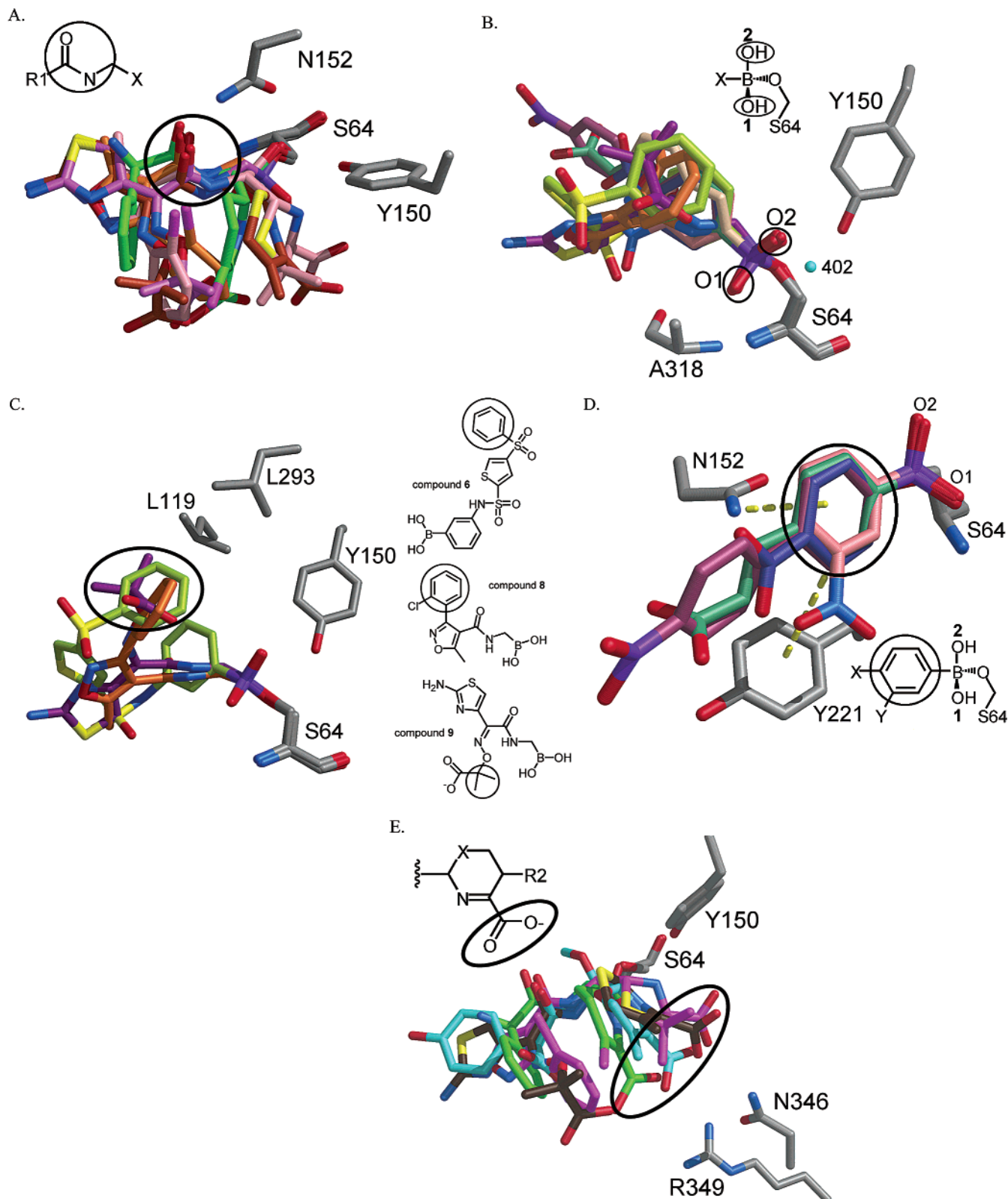
**Figure 3.** Binding sites identified experimentally on AmpC. (A) An amide binding site identified by superimposing all amide-containing compounds from Table 1. For clarity, only the structures of **8**−**12** are shown in this figure; these positions are representative of all other ligands determined. The amide group is circled in black. (B) Two hydroxyl binding sites identified by superimposing all boronic acid inhibitors. The hydroxyl sites are circled and labeled O1 and O2. (C) A hydrophobic binding site identified by superimposing the structures of **6**, **8**, **9**, **11**, and **12**; for clarity, only **6**, **8**, and **9** are shown. The hydrophobic binding site is composed of residues Leu119 and Leu293, and the hydrophobic portions of the compounds interacting with these residues are circled. (D) An aryl binding site identified by superimposing the structures of compounds **1**−**4**. Dashed yellow lines indicate the quadrupole interactions with Asn152 and Tyr221. (E) The carboxylate binding site identified by superimposing the structures of the β-lactams (**10**−**13**). The C3(4) carboxylate group is circled. Nitrogen atoms are colored blue, oxygens are colored red, sulfurs are colored yellow, chlorines are colored magenta, borons are colored purple, and carbons are colored gray, except for carbon atoms of the ligands, which are colored as follows: coral for **1**, indigo for **2**, sea green for **3**, violet for **4**, tan for **5**, lime green for **6**, gold for **7**, orange for **8**, magenta for **9**, green for **10**, brown for **11**, pink for **12**, and cyan for **13**.

**Table 4.** Comparison of Computationally Predicted Sites with Experimentally Determined Binding Sites in the AmpC Active Site

| | GRID[a] | | X-SITE[b] | | MCSS[c] |
| | site predicted? | | site predicted? | | site predicted? |
| experimental binding site | (apo) | (complex) | (apo) | (complex) | (complex) |
|---|---|---|---|---|---|
| R1 amide | yes | yes | yes | yes | no |
| O1 hydroxyl | no | no | no | no | yes |
| O2 hydroxyl | no | no | no | no | no |
| Leu119/Leu293 patch | yes | yes | yes | yes | no |
| Tyr221 | yes | yes | no | yes | no |
| Wat402 | no | no | no | no | no |
| Wat403 | no | yes | no | no | no |
| water in upper pocket (Wat404) | yes | yes | yes | yes | yes |
| water in lower pocket (Wat405) | yes | yes | no | no | yes |

[a] The contour levels for determining whether a site was predicted by GRID were −10 kcal/mol for all probes except the hydrophobic probe, where a contour level of −1.0 kcal/mol was used. [b] A site was successfully predicted by X-SITE if the closest probe position was <1.5 Å from the experimental site. [c] A site was successfully predicted by MCSS if a probe molecule ranked in the top 20% was also within 1.5 Å of the experimental site.

the $\beta$-lactams, **10**−**13**, in the AmpC/acyl−enzyme complexes made interactions characteristic of this site in $\beta$-lactam-recognizing enzymes.[20,30−34] Atom N$\delta$2 of Asn152 hydrogen bonds with the ligand amide oxygen in all of the complexes, although this distance is slightly long in the AmpC/**13** complex (3.3 Å). Atom N$\epsilon$2 of Gln120 interacts with the ligand amide oxygen only in the AmpC/**13** complex. The main chain oxygen of Ala318 interacts with the ligand amide nitrogen in the AmpC complexes with **10** and **13**. Three acylglycineboronic acid inhibitors, **7**−**9**, also contain an amide group in an equivalent position as the one found in the $\beta$-lactams. The amide groups of these compounds also made these characteristic interactions. Atom N$\delta$2 of Asn152 hydrogen bonds with the ligand amide oxygen in all of the complexes. The interaction between atom N$\epsilon$2 of Gln120 and the ligand amide oxygen is only observed in the AmpC/**7** complex. The interaction between the main chain oxygen of Ala318 and the ligand amide nitrogen is not observed in any of the boronic acid structures; however, in the AmpC/**8** complex, this distance is 3.3 Å.

How well is the amide recognition site predicted by the computational programs? GRID and X-SITE were tested with different starting conformations of AmpC, an apo and a complexed form. In the apo structure, the conformation of Gln120 is such that it hydrogen bonds with Asn152 and is better positioned to interact with the R1 amide group. In the complexed structure, Gln120 is swung out of the active site and no longer interacts with Asn152. In GRID, the trans amide probe successfully predicted this site in both conformations (Table 4). Starting with a complexed form of AmpC, a peak is observed near the nitrogen atom of the amide group at a contour level of −10 kcal/mol. Viewed at a slightly lower contour level (−9 kcal/mol), another peak appears near the position of the oxygen atom of the R1 amide group. Starting with the apo form of AmpC, both the nitrogen and the oxygen atoms of the R1 amide are predicted at a contour of −10 kcal/mol, and this site is the lowest energy minima overall (−15.5 kcal/mol). For X-SITE, the backbone N and backbone O probes were used to predict the amide site. The backbone N probe identified the amide nitrogen in both forms of AmpC. The amide oxygen was predicted by the backbone O probe only in the apo form. MCSS provided a large number of predictions ($N = 1018$) using the amide group probes (acw1, acw2, and acw3). A probe with an energy

of −7.18 kcal/mol did predict the correct position and orientation of the amide, but this was not one of the most energetically favorable predictions; it ranked 846, where a rank of 1 indicates the best energy probe position (Table 4).

**Carbonyl/Hydroxyl Binding Site.** A binding site that recognizes both carbonyl oxygens and hydroxyls was identified; this site corresponds to the "oxyanion"[35] or "electrophilic"[6] hole of AmpC. Two hydroxyl groups, O1 and O2, are displayed as part of the boronic acid portion of **1**−**9** (Figure 3B), and in each of the structures, the hydroxyls make characteristic interactions with the enzyme (Table 3). The O1 hydroxyl always interacts with the main chain nitrogens of Ser64 and Ala318, acting as an acceptor. O1 also appears to donate its proton to form a hydrogen bond with the main chain oxygen of Ala318 (Figure 3B). The carbonyl oxygen of the $\beta$-lactams (**10**−**13**) was also observed to bind in this site. For the complexes with **10** and **13**, the lactam carbonyl oxygen hydrogen bonds with the main chain nitrogens of Ser64 and Ala318. In addition to interactions with these nitrogens, a close contact to the main chain oxygen of Ala318 is observed in the complexes with **11** and **12**.

**Hydroxyl Binding Site.** An additional binding site for hydroxyl groups was also identified (Figure 3B). The other boronic acid hydroxyl, O2, of **1**−**9** also makes characteristic interactions with the enzyme (Table 3). The O2 hydroxyl hydrogen bonds with Tyr150 and a water molecule, Wat402.

Neither hydroxyl binding site was identified computationally by GRID or X-SITE, owing to the close proximity of Ser64O$\gamma$ to the O1 and O2 hydroxyls of the boronic acid (Table 4). Contouring at very low levels in GRID resulted in a cage forming around the O$\gamma$ atom, showing that probes would not be predicted to bind within the van der Waals radius of this atom. MCSS did not identify the O2 site but did correctly identify the O1 hydroxyl site. A methanol probe (ranked 36 out of 199 possible) was positioned such that it interacted with the main chain nitrogen and oxygen atoms of Ala318, and its RMSD from the experimental position of the O1 hydroxyl was 0.6 Å.

**Hydrophobic Binding Site.** Another binding site identified on AmpC recognizes hydrophobic groups. This site is composed of residues Leu119 and Leu293, which form a hydrophobic patch in the active site. Phenyl rings were observed to form van der Waals interactions with

these residues, as observed in the complexes of AmpC with **6**, **8**, and **12**[20,24,26] (Table 1; Figure 3C). In the complexes of AmpC with the $\beta$-lactams **10** and **13**, the carbacephem and oxacephem rings, respectively, interact with the leucines.[20] In other structures, a methyl group is within van der Waals distance to these residues, as with **9** and **11**[33] (Figure 3C).

GRID and X-SITE predicted this hydrophobic binding site (Table 4). In GRID, the "dry" probe correctly identified this site in both forms of AmpC (contour $-1.0$ kcal/mol). The aromatic ring CH probe was used in X-SITE and also identified this site in both forms of the enzyme. In MCSS, the benzene probe was used to predict this site. Seventy-five positions for this probe were observed in the active site overall, and the probe nearest to the Leu119/Leu293 binding site was ranked 55. None of the probes ranked in the top 20% were within 1.5 Å of the experimental site.

**Aryl Quadrupole Binding Site.** The structures of the arylboronic acid inhibitors, **1**−**6**, revealed a binding site for the aryl rings present off the boronic acid group (Figure 3D). On the basis of visualization of the structures, the aryl rings appear to form quadrupole−dipole interactions with Asn152, with distances between 3.6 and 3.7 Å (Table 3). Similarly, the aryl rings stack in a herringbone fashion with Tyr221, appearing to form quadrupole−quadrupole interactions with this residue (distances ranged from 4.2 to 5.0 Å; Table 3). We note that we have not explored the exact nature of this interaction by anything more sophisticated than geometry of approach in the crystal structures.

Is this aryl binding site predicted computationally? The same hydrophobic probes used to identify the Leu119/Leu293 site were used to predict this site. This site was successfully predicted by GRID (Table 4); in the complexed structure, this site was the lowest energy minimum for the active site region, with an energy of $-2.09$ kcal/mol. X-SITE predicts this site only in the complexed conformation of AmpC. In MCSS, one of the benzene ring predictions overlays closely with the aryl ring from the AmpC/**5** structure (RMSD 0.9 Å); however, it is not one of the lowest energy predictions (ranked 41 out of 75).

**Primary Carboxylate Binding Site.** $\beta$-Lactams contain a carboxylate group at the C3(4) position of the ring fused to the lactam core. The structures of the AmpC/$\beta$-lactam acyl−adduct complexes (**10**−**13**) reveal a carboxylate binding site formed by Asn346 and Arg349 (Table 1, Figure 3E). The C4 carboxylate group of **10** (loracarbef) interacts with residues Asn343, Asn346, and Arg349 via water molecules.[20] In AmpC/**11** (ceftazidime), this carboxylate interacts directly with Asn346 and via a water molecule with Arg349.[33] The carboxylate of **12** (cloxacillin) interacts directly with Asn346 and with Arg349 via a water molecule. In this structure, the carboxylate also hydrogen bonds with Thr316.[20] In the AmpC/**13** (moxalactam) complex, the C4 carboxylate hydrogen bonds directly with Asn289 and Asn346 and interacts, via water molecules, with Asn343 and Arg349.[20] None of the computational programs were used to predict carboxylate binding sites on AmpC.

**Secondary Carboxylate Binding Site.** All $\beta$-lactams contain a carboxylate at their C3(4) positions, and so it is not surprising that there is a carboxylate

recognition site on AmpC. Some $\beta$-lactams also contain a second carboxylate on their R1 side chains (e.g., **11** and **13**), and we were interested to see if there was a consensus position for a secondary carboxylate group. The carboxylate groups on the arylboronic acid inhibitors **2** and **3** also probed for such a site in the R1 region of the active site. In the AmpC/**2** complex, the carboxylate group may interact with Gln120 in molecule 1 (Gln120N$\epsilon$2−OX1 = 3.3 Å). In molecule 2, this distance is 2.9 Å because Gln120 is in a different conformation. The carboxylate group found in **3** interacts only with a single water molecule in the site. The secondary carboxylate group found on the $\beta$-lactam ceftazidime (**11**) and the analogous carboxylate on **9** is exposed to bulk solvent and makes no specific interactions with AmpC. The secondary carboxylate on moxalactam (**13**) interacts with a single water molecule in the site. The lack of specific interactions between AmpC and carboxylates in the R1 site suggests that a carboxylate binding site is not explicitly defined in this region.

**Water Binding Sites.** For all of the structures used in this study, the total number of water molecules ranged from 95 (for the AmpC/**5** complex, determined to 2.25 Å resolution) to 500 (for the AmpC/**8** complex, determined to 1.75 Å resolution). In the 15 structures, AmpC is observed in 30 different environments, since there are two molecules of AmpC present per asymmetric unit. Six water sites are conserved in all 30 molecules studied here to within 1 Å (see Table 1 of Supporting Information). All of these six sites are conserved between molecule 1 and molecule 2 of the higher resolution apo AmpC structure (PDB entry 1KE4); in total, 95 water molecules are conserved between the two molecules of the 1KE4 structure. An additional 11 water sites are conserved in 29 of the structures; eight more are in 28, and six are in 27. Approximately half of these consensus water sites (16 out of 31) was buried from the bulk solvent, with solvent accessibilities of less than 1%. Among the 31 consensus waters, three are found in the active site region of AmpC. One of these is Wat403, which hydrogen bonds with Asn346 and Arg349. The other two, Wat404 and Wat405, each occupy one of two observable pockets adjacent to the R1 site (Figure 1). These pockets are composed of conserved residues. Ala215 and Tyr221 form the upper pocket, where Wat404 is bound, and Glu61, Thr319, and Phe322 form the lower pocket, where Wat405 is bound.

In the apo active site of AmpC, several other waters are observed (Figure 2). We wondered if any of these water molecules defined ligand binding sites. One of these waters is Wat402, the presumed deacylating water molecule. It hydrogen bonds with O$\gamma$1 of Thr316 and conserved Wat403. Wat402 is observed in 22 of the 30 molecules, and this includes all nine of the AmpC/boronic acid complexes in which Wat402 also hydrogen bonds with the O2 hydroxyl of the boronic acid. Three other active site waters (Wat768, Wat715, and Wat770) corresponded with ligand atom positions from the crystal structures. Wat768 is bound in the oxyanion/electrophilic hole and interacts with the main chain nitrogen atoms of Ser64 and Ala318 and the main chain oxygen of Ala318. This corresponds to the position of the O1 hydroxyl of the boronic acids and the carbonyl

oxygens of the β-lactam acyl–enzyme complexes. Wat715 is 2.7 Å from the main chain oxygen of Ala318 and occupies a position similar to that of the nitro group oxygen in the AmpC/**1** complex (0.9 Å) and the sulfonamide oxygen in the AmpC/**6** complex (1.1 Å). Wat770 is observed near the position of the dihydrothiazine or penicillanic rings of the acylated β-lactams; it is 1.8 Å from the sulfur atom in ceftazidime (**11**), 0.3 Å from the sulfur atom in cloxacillin (**12**), and 1.2 Å from the oxacephem ring oxygen atom in moxalactam (**13**).

Finally, how well do the computational programs predict the water binding sites observed crystallographically? GRID alone predicted the position of Wat403 but only in the complexed form of AmpC. The water molecules found in the upper and lower pockets (Wat404 and Wat405, respectively) were predicted by GRID in both the complexed and the apo forms of AmpC. X-SITE identifies the water in the upper (Wat404) but not the lower (Wat405) pocket. Conversely, MCSS predicts the water in the lower (ranked five out of 116) but not the upper pocket. Wat402 was not predicted by any of the programs, possibly because it makes only a single hydrogen bond with the protein, to Oγ1 of Thr316. Wat402 does interact with ligands bound in the active site, for example, the O2 hydroxyl of the boronic acid inhibitors (Table 3) or the lactam nitrogens in several of the β-lactam acyl–enzyme structures. Interestingly, Wat402 is observed in the crystal structure of the apo AmpC structure but with higher *B* factors as compared to the average *B* factor of all waters (48.8 vs 35.6 Å²). The solvent accessibility to this site is slightly greater than for Wat403 (13.4 vs 9.8%). As for the rest of the 31 consensus waters, GRID predicted 20 of the remaining 28 water sites, starting with the apo conformation of AmpC, and 21 out of 28 with the complexed conformation. With X-SITE, only seven of the remaining 28 consensus water sites were present in the defined active site region, and X-SITE predicted only one of the seven to within 1 Å, starting with the apo conformation, and none when starting with the complexed form. For MCSS, only 15 of the remaining consensus water sites were included in the active site sphere used in the calculation, and MCSS predicted six of the 15 to within 1 Å.

**Novel Binding Sites Predicted Computationally.** We were also interested in binding sites predicted by at least two of the three computational programs that were not identified in the consensus overlay of inhibitor complexes. Four potential binding site hot spots were identified this way: three novel amide binding sites and one new hydrophobic site (Figure 4). First, all of the programs suggested that an amide group would favorably bind in the upper pocket, near Wat404. Second, GRID and MCSS predicted an amide site inside the tunnel near residues Arg148 and Glu272. A third amide site was identified by GRID and MCSS at the entrance to the tunnel near residues Ser64 and Tyr150. This site corresponds to the location of the C4 carboxylate group in the AmpC/**11** (ceftazidime) structure. X-SITE predicted a nitrogen probe midway between these latter two sites. The tunnel and the entrance to the tunnel were also predicted by GRID and MCSS as binding sites for water and hydroxyl functional groups. A novel hydrophobic site on AmpC near Trp93, Ala160, Leu161,
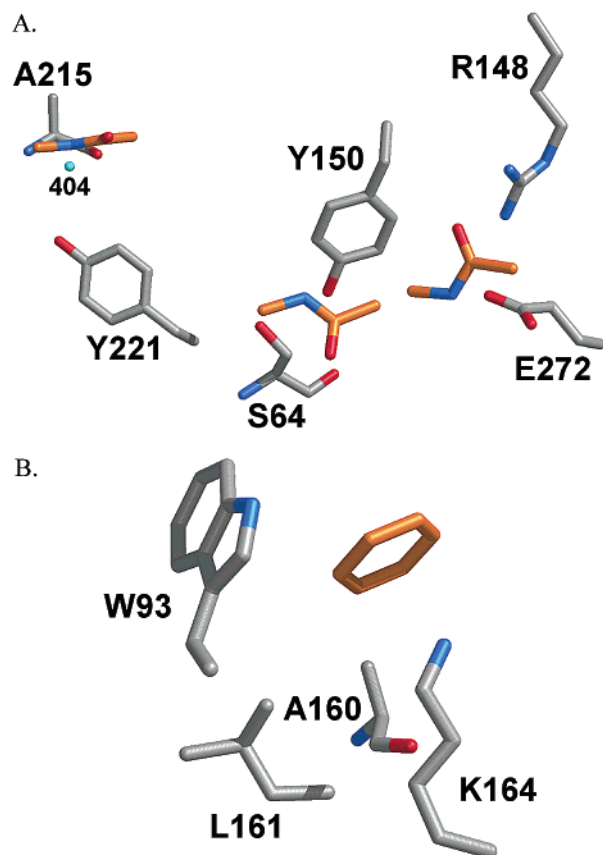


**Figure 4.** Novel binding sites identified on AmpC by GRID, X-SITE, and MCSS. (A) Three novel amide binding sites. (B) A novel hydrophobic binding site. A representative functional group molecule, with carbon atoms colored orange, is placed in each novel site identified.

and Lys164 was predicted by GRID and MCSS. This site was approximately 20 Å from Ser64 and located on the surface of the enzyme. GRID identified this site as the lowest energy minimum overall in the apo structure; in MCSS, this site was occupied by the number one ranked benzene probe. This site was outside the region studied with X-SITE.

## Discussion

**Experimentally Identified Binding Sites on AmpC.** There are several functional groups found in all β-lactams, including the lactam carbonyl group, the C3-(4) carboxylate functionality, and the C6(7)-β-amide that makes up the proximal part of the R1 side chain of these antibiotics (**10–13**, Table 1). Not surprisingly, these functionalities find well-conserved complements in the AmpC active site that are readily apparent in the consensus overlay of ligand complexes (Figure 5). As observed in every serine β-lactam-recognizing enzyme studied,[4,30,36–41] there is a well-conserved oxyanion[35] or electrophilic[6] hole that recognizes the carbonyl oxygen of the lactam acyl adduct, made up of the main chain atoms of Ser64 and Ala318 in AmpC. The C3(4) carboxylate is recognized by Asn346 and Arg349. The C6-(7)-β-amide of the R1 side chain is recognized by the conserved Asn152 of AmpC. The conserved Gln120 and the main chain oxygen of Ala318 also contribute to recognizing this ligand group, although these interactions are much less conserved in the consensus overlay than that of Asn152.
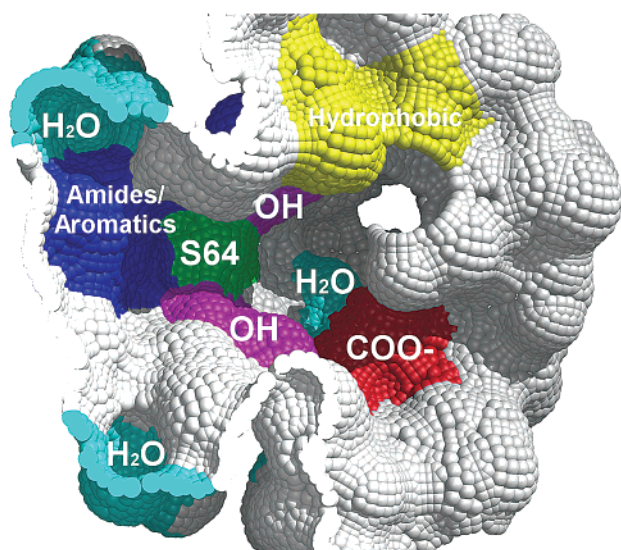
**Figure 5.** Integrated map of the AmpC active site. Binding sites identified experimentally from the crystal structures are colored as follows: the amide/aromatic site, blue; the hydrophobic site, yellow; the C3(4) carboxylate site, red; the hydroxyl sites, magenta; and the water sites, cyan. The catalytic residue Ser64 is colored green.

Several surprising binding site hot spots that would not be predicted from looking at individual β-lactam substrates and inhibitors also emerged from the consensus overlay. In addition to substrate carbonyl oxygens, the oxyanion[35] or electrophilic[6] hole also recognizes hydroxyl groups. In every AmpC/boronic acid complex, the O1 hydroxyl of the inhibitor binds in this site, making the same interactions with the enzyme as the carbonyl oxygen of the β-lactams. In contrast to an apparently unfavorable close contact between the carbonyl oxygens of several β-lactams and the Ala318, the O1 hydroxyl can act as a hydrogen bond donor with the main chain oxygen of Ala318, thereby making an additional favorable interaction in this site. The identification of a second hydroxyl binding site was interesting from a mechanistic perspective. This site is defined by the O2 hydroxyl of the boronic acids inhibitors, which mimic the tetrahedral transition state. In complexes with this class of inhibitors, O2 is thought to represent the position of the deacylating water in the deacylation transition state. This hydroxyl makes two hydrogen bonds in all of the complexes: one with Tyr150, the suggested general base in the reaction,[4,11,23] and the other with Wat402, the presumed deacylating water. Wat402 is observed in all of the boronic acid complexes and suggests the direction of attack of the hydrolytic water on the carbonyl carbon of the acyl adduct. The O2 hydroxyl site was not predicted by the computational programs, and MCSS was the only program to predict the O1 site. In the AmpC/boronic acid complexes, the positions of O1 and O2 are determined by the covalent attachment of this class of inhibitors to Ser64. In the complexes, these atoms might be so close to Ser64Oγ as to make these positions difficult to predict.

Unexpectedly, we observed that an aryl ring could replace the amide group by making alternate interactions with some of the amide-recognizing residues. In the AmpC/arylboronic acid complexes, the aryl ring of the inhibitor makes quadrupole−dipole interactions with Nε2 of the conserved residue Asn152 and quadru-

pole−quadrupole interactions with Tyr221. Distal portions of the boronic acid inhibitors can displace Gln120, causing it to swing away from the binding site. On the other hand, atom Nε2 of Asn152 appears to track with the center of the aryl ring to maintain its interaction in each of the AmpC/arylboronic acid complexes. There is clearly some plasticity to ligand recognition by AmpC; a completely conserved residue, essential for enzyme function, can form different interactions and recognize ligand functionalities unrelated to the substrate. Such plasticity might be useful for inhibitor design.

The computational predictions did surprisingly well at characterizing this unexpected site. GRID predicts a hydrophobic binding site in this region, although it is difficult to say whether the quadrupole−dipole interaction is being captured or simply stacking with the adjacent Tyr221. X-SITE also predicts an aromatic carbon probe in this site but only in the complexed conformation of the enzyme. With MCSS, an aryl ring binding site was predicted near the location of the aryl ring of **5** (RMSD 0.9 Å), but it is not one of the most energetically favorable sites (ranked 41 out of 75).

A hydrophobic binding site formed by conserved residues Leu119 and Leu293 was also identified by the consensus superpositions. Phenyl rings and methyl groups made van der Waals interactions with these residues. Also, the carbacephem and oxacephem rings of the β-lactams **10** and **13** also interacted here. Computationally, GRID and X-SITE both predicted this hydrophobic site.

In considering these consensus binding sites, it is appropriate to note that four of the ligands that contribute to them, the β-lactams **10**−**13**, are irreversible, covalent modifiers of AmpC, and meaningful binding energies cannot be measured. How trustworthy, then, are the binding sites that emerge from overlaying these molecules? Individually, any given complex of one of these molecules identifies a binding site with only modest confidence. The advantage of the consensus overlay of the four β-lactams, along with the nine boronic acids, is that the functionalities common to all four irreversible compounds are observed to bind in the same regions of the site. This suggests that the areas identified are favorable binding regions for this type of functionality, irrespective of the overall binding energy of the entire molecule on which they are found. Moreover, several of the functional groups, such as the R1 amide side chain and the nonpolar groups that bind to the leucine hydrophobic patch, are also found in the nine boronic acid inhibitors, which are genuine reversible inhibitors of AmpC. These groups, common to both the boronic acids and the β-lactams, bind in the same regions of the active site.

The relative energetic contributions made by the binding of the characteristic ligand functionalities to the consensus sites that they define can be estimated. The boronic acids are competitive, reversible inhibitors of AmpC, and their binding energies can be calculated from their $K_i$ values.[42] By comparing the $K_i$ values of related inhibitors, it can be shown that for the R1 side chain amide of the acylglycineboronic acids, and by extension β-lactams, binding in the amide site contributes 3.2 kcal/mol in affinity.[24] Similarly, the aryl ring in the aryl recognition site appears to contribute 100−

1000-fold (2.8–4.2 kcal/mol) to affinity.[43] In the crystal structures, this increase in affinity is attributed to the quadrupole interactions observed between the aryl ring at this position and the residues Asn152 and Tyr221. Groups that bind to the hydrophobic binding site formed by Leu119 and Leu293 are more difficult to estimate based on the inhibitors we have studied, but they may account for 10–100-fold increases in affinity, depending on the ligand functionality.[26,33] The energetic contribution of the primary carboxylate site of $\beta$-lactams has only begun to be investigated for AmpC, but on the basis of studies of class A $\beta$-lactamases, this site may contribute 3–4 orders of magnitude in binding affinity.[24,44,45] The contribution of the carbonyl/hydroxyl binding sites is not possible to estimate due to the covalent mechanism of the $\beta$-lactams and the inability to uncouple the contributions of the hydroxyls from those of the boron in the boronic acids. Nevertheless, these binding sites appear to be regions of favorable energetic complementarity to AmpC.

**Computational Binding Site Predictions.** How accurate is the experimental consensus binding site map of AmpC, and how well did the theoretical predictions correspond with it? The X-ray structures varied in resolution from 1.72 (for the apo structure) to 2.46 Å (for the cloxacillin complex). On the basis of standard Luzzati analysis,[46] the corresponding errors in position vary from 0.2 to 0.3 Å RMS. These values probably underestimate the uncertainty in the placement of a binding site, however. A more conservative estimate may be taken from the variations in the relative positions of the consensus binding sites themselves, based on an overlay of all of the structures used to predict them. Representative of the variations in the consensus binding locations of the inhibitor functional groups were an RMS deviation of 0.16 Å for the O1 hydroxyl positions of the boronic acids and an RMS deviation of 0.73 Å for the amide oxygen atoms of the R1 amide site.

The sites predicted by GRID corresponded best with the experimental structures. Starting with the complexed form of AmpC, it successfully predicted most of the experimental binding sites that we examined, except for Wat402 and the O1 and O2 hydroxyls, the latter two of which we would not have expected it to predict. Additionally, predictions for the R1 amide site (apo) and the Tyr221 site (complex) were located at the lowest energy minima overall. MCSS predicted probes for every site, using a 2.0 Å RMSD cutoff. However, the MCSS probes with the best RMSD were rarely the most energetically favorable. Typically, the majority of site predictions for a particular probe ranked higher than the experimental configuration; the only predicted sites that also ranked in the top 20% were those of the O1 hydroxyl and Wat405. X-SITE predicted the hydrophobic sites, the amide site (the amide nitrogen better than the amide oxygen), and one of the conserved water molecule positions (Wat404).

How sensitive were these methods to the starting conformation of the enzyme? The computational calculations with GRID and X-SITE were performed on two different starting targets (apo vs complexed AmpC). The resulting predictions differed somewhat, suggesting that there was some dependence on the starting target used.

The R1 amide site was better predicted when starting with the apo structure, and this site was identified as the overall lowest energy minimum for this type of probe with GRID. The water sites were better predicted by GRID when using the complexed structure as a starting model. The Leu119/Leu293 hydrophobic site was predicted equally well with either starting structure. The Tyr221 hydrophobic site was also identified by GRID in both the apo and the complexed forms. However, this site was better predicted with the complexed form of the enzyme, where GRID predicts the Tyr221 site as the overall lowest energy minima, and X-SITE only predicts this site when using the complexed conformation.

In addition to a comparison of the computational predictions with the experimentally determined binding sites, it is interesting to consider whether hot spots are predicted that are not observed in the experimental structures. For instance, the two pockets defined by the ordered waters Wat404 and Wat405 and the tunnel that runs through the enzyme simply look like binding sites; despite the fact that no ligand is known to bind to these sites, the residues that define them are highly conserved (Figure 1). We therefore considered novel sites predicted by at least two of the three computational programs. All three programs predict an amide as a high-scoring group in the pocket defined by Wat404 (Figure 4A)—this was the highest scoring position for an amide predicted by GRID. GRID and MCSS predicted another amide site inside the AmpC tunnel near Arg148 and Glu272 and an amide/hydroxyl site at the entrance of the tunnel near Ser64 and Tyr150 (Figure 4A). Both programs found a hydrophobic binding site 20 Å distant from the active site, in the region of Trp93, Leu161, and Lys164 (Figure 4B). Although this site is unlikely to be useful for ligands directed to the active site, we note that this region has been observed to bind cephalosporin antibiotics as a secondary binding site (Beadle, Minasov, and Shoichet, unpublished). Irrespective of the function, if any, of these putative sites, these consensus predictions suggest that they would be sensible to explore for ligand design and discovery.

The consensus map that emerges from this study (Figure 5) is made up of groups contributed by different molecules. No single ligand binds to all of the hot spots identified. In principle, it is possible to imagine a molecule that spans all of the consensus sites. Assuming additivity, such an imaginary molecule would pick up as much as 3–4 kcal/mol at each site, leading to a much more active reversible inhibitor than the best identified to date for AmpC, which has a $K_i$ value of 20 nM.[24] Whether such a molecule is synthetically feasible is unclear at this point. Putting synthesis of such an über inhibitor aside, the consensus binding sites can be linked together to construct a pharmacophore that may be a useful starting point in the design and synthetic elaboration of novel inhibitors for AmpC. Similarly, this consensus map can be used as target sites in a molecular docking screen of a database of small molecules to identify leads that contain the functionalities known to favorably bind in the active site. Indeed, several groups[21,24,47,48] are actively pursuing these and related lines of investigation for $\beta$-lactamases. More generally, this approach might be applied to other enzymes that

are amenable to structural methods and for which an understanding of binding site hot spots is desired.

## Experimental Section

**Crystal Growth and Structure Determination.** AmpC from *Escherichia coli* was expressed and purified to homogeneity, as described.[6] Compound **1** was obtained from Aldrich Chemical, Milwaukee, WI. Compounds **2**−**4** were obtained from Lancaster Synthesis, Windham, NH. Cocrystals of AmpC with **1**−**4** were grown by vapor diffusion in hanging drops over 1.7 M potassium phosphate buffer (pH 8.7) using microseeding techniques. For all, the initial concentration of protein in the drop was 95 $\mu$m. The concentration of **1**, **3**, and **4** in the drops was 590 $\mu$M, and the concentration of **2** was 485 $\mu$M. Compounds **3** and **4** were added to the drop in a 2% dimethyl sulfoxide (DMSO), 1.7 M potassium phosphate buffer (pH 8.7) solution; **1** and **2** were dissolved in 1.7 M potassium phosphate buffer (pH 8.7) before they were added to the drop. Crystals were grown at 23 °C and appeared within 3−5 days.

The data collection protocols for the structures of native AmpC and AmpC in complexes with **1**−**4** were as follows. For the native AmpC structure, data were collected on the DND-CAT beam line (5IDB) of the Advanced Photon Source at Argonne National Lab at 100 K using a 162 mm Mar CCD detector. Prior to data collection, the native crystal was immersed in a cryoprotectant solution of 20% sucrose, 1.7 M potassium phosphate, pH 8.7, for about 20 s, and then flash cooled in liquid nitrogen. The data were measured from a single crystal. For AmpC/**1**, the cocrystal was mounted in a silanized glass capillary and allowed to equilibrate for 3 days before data collection. Data were measured on an R-Axis-IIC image plate system at room temperature from a single crystal. For AmpC/**2**, the cocrystal was harvested using a nylon loop and immersed in a cryoprotectant solution of 20% sucrose, 1.7 M potassium phosphate, pH 8.7, for about 30 min and then flash cooled in the cold stream. Data were measured on an R-Axis-IIC image plate system at 100 K from a single crystal. For AmpC/**3** and AmpC/**4**, each cocrystal was harvested using a nylon loop and immersed in a cryoprotectant solution of 20% sucrose, 1.7 M potassium phosphate, pH 8.7, for about 20 s and then flash cooled in liquid nitrogen. Each data set was measured on an R-Axis IIC image plate system at 100 K from single crystals. The structures of AmpC with compounds **5**−**13** have all been reported previously (see Table 1 for details).

For all structures, reflections were indexed, integrated, and scaled using the HKL package[49] (Table 2). The space group was $C2$, with two AmpC molecules in the asymmetric unit. For AmpC/**1**, AmpC/**2**, AmpC/**3**, and AmpC/**4**, each AmpC molecule contained 358 residues. For the native structure, molecule 2 of the asymmetric unit contained 358 residues, and molecule 1 contained 352 residues; residues 285−290 were excluded from the final model due to poor electron density in this region. The structures of AmpC/**1**, AmpC/**2**, AmpC/**3**, and AmpC/**4** were determined using molecular replacement with a boronic acid complexed structure (PDB entry 1C3B),[25] with inhibitor and water molecules removed, as the initial phasing model. The model of AmpC/**1** was refined entirely with X-PLOR,[50] which included a bulk solvent correction and a 2.0 $\sigma$ cutoff. Models of AmpC/**2**, AmpC/**3**, and AmpC/**4** were refined initially with X-PLOR, including a bulk solvent correction and a 2.0 $\sigma$ cutoff. Initial difference electron density maps were calculated with X-PLOR, and the inhibitors were built into the observed difference density in each active site of the asymmetric unit. The structures of the complexes (AmpC/**2**, AmpC/**3**, or AmpC/**4**) were further refined using the maximum likelihood target in CNS[51] and included a bulk solvent correction and a 2.0 $\sigma$ cutoff (Table 2). $\sigma$A-weighted electron density maps were calculated using CNS and used in steps of manual rebuilding using O.[52]

The native AmpC structure was determined by molecular replacement using a previously determined native AmpC structure (PDB entry 2BLS)[6] as the initial phasing model with water molecules removed. Two-fold noncrystallographic symmetry averaging was used to improve the initial electron density maps using the program RAVE.[53,54] After manual fitting with O,[52] the model was refined using CNS, imposing strict NCS constraints. Two rounds of model building into averaged maps were performed. Afterward, the NCS constraints were released, and the model was further refined with CNS.

**Computational Binding Site Prediction Programs.** GRID and X-SITE calculations were performed on the structures of apo AmpC (molecule 2 of PDB entry 1KE4) and complexed AmpC (molecule 2 of AmpC/**8**; PDB entry 1FSY).[24] The complexed and apo forms of AmpC were used to observe any differences that might arise in the predictions due to the starting model. Additionally, they represent two conformations of the flexible residue Gln120. In the apo form, Gln120 is close to the active site and interacts with Asn152. In the complexed form, Gln120 has swung out of the active site and interacts with residues in a crystallographic symmetry mate. MCSS calculations were performed only on a complexed structure (AmpC/**5**; PDB entry 1C3B).[25] In this structure, Gln120 is swung out of the active site. All inhibitor atoms, water molecules, and phosphate ions were removed from each structure prior to the calculations. The calculations were performed on each molecule in the asymmetric unit separately.

**GRID Version 18.** Prior to running GRID, the net charge on AmpC was neutralized for the complexed and apo structures, substituting the surface residues Lys84, Lys99, and Lys239 with alanines in the coordinate file. The structures were prepared for use in GRID with the program GRIN and the data file GRUB.[17] The parameters in GRUB are based on the "extended" atom concept[55] used for CHARMM. The probes used to identify binding sites in the active site region of AmpC were water, "dry" (or hydrophobic), hydroxyl, and trans amide group. For calculations involving the active site region, a grid spacing of 0.25 Å was used. The active site region for the apo structure was defined as a box with dimensions of 29 × 29 × 24 Å³ and centered at the Cα atom of Ala220. For the complexed structure, the box was centered at the Cα atom of Ala220 with dimensions of 29 × 28 × 26 Å³. The water probe was also used to probe an entire molecule of AmpC to identify binding sites further away from the active site. For this calculation, a larger grid spacing of 0.5 Å was used. Contouring the energy maps at different levels allowed for visualization of the signal-to-noise ratio. Except for the hydrophobic probe, an energy contour of −10 kcal/mol was found to be appropriate for distinguishing strong peaks of predicted binding sites. For the hydrophobic probe, an energy contour of −1 kcal/mol was used.

**X-SITE Version 1.0.** Binding site predictions were calculated for 25 probe molecules and limited to the active site region of AmpC. This region was determined using the GENBOX program in SURFNET (version 1.4).[56] The center of this region was given as the C$\beta$ atom of Tyr221 and defined as a box surrounding the active site with dimensions of 25 × 25 × 25 Å³.

**MCSS.** To prepare the AmpC structure for use with MCSS, hydrogens and lone pairs were added in InsightII (Accelrys, San Diego, CA) using the CHARMm 22 force field (pH 7.0). The active site was defined as a sphere with its center at O$\gamma$ of Ser64 and a radius of 17.5 Å. All functional groups were tested, but only the water (watr), benzene (benz), hydroxyl (meoh), and amide groups (acw) were analyzed in depth. Five iterations of the following procedure were performed for each functional group. The site was filled with 500 copies of each functional group, and minimization was performed using a steepest descent algorithm. Default parameters were used for the dielectric. Functional groups that converged to the same minima were eliminated based on an RMS cutoff of 0.2 Å.

**Analysis of Water Sites.** Identification and solvent accessibilities of conserved water sites in the structures were performed with the program EDPDB.[57] Molecule 2 of the native apo structure (PDB entry 1KE4) was the reference to which all other structures were compared. Both molecules of each of the 14 structures in Table 1 and both molecules of native apo AmpC (PDB entry 1KE4) were used in the analysis.

**Supporting Information Available:** Table of conservation of water molecules in the AmpC complexes. This material is available free of charge via the Internet at http://pubs.acs.org.

## References

(1) Bennett, P. M.; Chopra, I. Molecular basis of beta-lactamase induction in bacteria. *Antimicrob. Agents Chemother.* **1993**, *37*, 153−158.

(2) Jacobs, C.; Frere, J. M.; Normark, S. Cytosolic intermediates for cell wall biosynthesis and degradation control inducible beta-lactam resistance in gram-negative bacteria. *Cell* **1997**, *88*, 823−832.

(3) Hanson, N. D.; Sanders, C. C. Regulation of inducible AmpC beta-lactamase expression among Enterobacteriaceae. *Curr. Pharm. Des.* **1999**, *5*, 881−894.

(4) Oefner, C.; D'Arcy, A.; Daly, J. J.; Gubernator, K.; Charnas, R. L.; et al. Refined crystal structure of beta-lactamase from *Citrobacter freundii* indicates a mechanism for beta-lactam hydrolysis. *Nature* **1990**, *343*, 284−288.

(5) Lobkovsky, E.; Moews, P. C.; Liu, H.; Zhao, H.; Frere, J. M.; et al. Evolution of an enzyme activity: crystallographic structure at 2-A resolution of cephalosporinase from the ampC gene of *Enterobacter cloacae* P99 and comparison with a class A penicillinase. *Proc. Natl. Acad. Sci. U.S.A.* **1993**, *90*, 11257−11261.

(6) Usher, K. C.; Blaszczak, L. C.; Weston, G. S.; Shoichet, B. K.; Remington, S. J. Three-dimensional structure of AmpC beta-lactamase from *Escherichia coli* bound to a transition-state analogue: Possible implications for the oxyanion hypothesis and for inhibitor design. *Biochemistry* **1998**, *37*, 16082−16092.

(7) Crichlow, G. V.; Kuzin, A. P.; Nukaga, M.; Mayama, K.; Sawai, T.; et al. Structure of the extended-spectrum class C beta-lactamase of *Enterobacter cloacae* GC1, a natural mutant with a tandem tripeptide insertion. *Biochemistry* **1999**, *38*, 10256−10261.

(8) Tsukamoto, K.; Tachibana, K.; Yamazaki, N.; Ishii, Y.; Ujiie, K.; et al. Role of lysine-67 in the active site of class C beta-lactamase from *Citrobacter freundii* GN346. *Eur. J. Biochem.* **1990**, *188*, 15−22.

(9) Dubus, A.; Wilkin, J. M.; Raquet, X.; Normark, S.; Frere, J. M. Catalytic mechanism of active-site serine beta-lactamases: role of the conserved hydroxy group of the Lys-Thr(Ser)-Gly triad. *Biochem. J.* **1994**, *301*, 485−494.

(10) Dubus, A.; Normark, S.; Kania, M.; Page, M. G. Role of asparagine 152 in catalysis of beta-lactam hydrolysis by *Escherichia coli* AmpC beta-lactamase studied by site-directed mutagenesis. *Biochemistry* **1995**, *34*, 7757−7764.

(11) Dubus, A.; Ledent, P.; Lamotte-Brasseur, J.; Frere, J. M. The roles of residues Tyr150, Glu272, and His314 in class C beta-lactamases. *Proteins: Struct., Funct., Genet.* **1996**, *25*, 473−485.

(12) Ringe, D. What makes a binding site a binding site? *Curr. Opin. Struct. Biol.* **1995**, *5*, 825−829.

(13) Minke, W. E.; Diller, D. J.; Hol, W. G.; Verlinde, C. L. The role of waters in docking strategies with incremental flexibility for carbohydrate derivatives: heat-labile enterotoxin, a multivalent test case. *J. Med. Chem.* **1999**, *42*, 1778−1788.

(14) Allen, K. N.; Bellamacina, C. R.; Ding, X. C.; Jeffery, C. J.; Mattos, C.; et al. An experimental approach to mapping the binding surfaces of crystalline proteins. *J. Phys. Chem.* **1996**, *100*, 2605−2611.

(15) Nienaber, V. L.; Richardson, P. L.; Klighofer, V.; Bouska, J. J.; Giranda, V. L.; et al. Discovering novel ligands for macromolecules using X-ray crystallographic screening. *Nat. Biotechnol.* **2000**, *18*, 1105−1108.

(16) Shuker, S. B.; Hajduk, P. J.; Meadows, R. P.; Fesik, S. W. Discovering high-affinity ligands for proteins: SAR by NMR. *Science* **1996**, *274*, 1531−1534.

(17) Goodford, P. J. A computational procedure for determining energetically favorable binding sites on biologically important macromolecules. *J. Med. Chem.* **1985**, *28*, 849−857.

(18) Miranker, A.; Karplus, M. Functionality maps of binding sites: a multiple copy simultaneous search method. *Proteins: Struct., Funct., Genet.* **1991**, *11*, 29−34.

(19) Laskowski, R. A.; Thornton, J. M.; Humblet, C.; Singh, J. X-SITE: use of empirically derived atomic packing preferences to identify favourable interaction regions in the binding sites of proteins. *J. Mol. Biol.* **1996**, *259*, 175−201.

(20) Patera, A.; Blaszczak, L. C.; Shoichet, B. K. Crystal structures of substrate and inhibitor complexes with AmpC beta-lactamase: Possible implications for substrate- assisted catalysis. *J. Am. Chem. Soc.* **2000**, *122*, 10504−10512.

(21) Crichlow, G. V.; Nukaga, M.; Doppalapudi, V. R.; Buynak, J. D.; Knox, J. R. Inhibition of class C beta-lactamases: structure of a reaction intermediate with a cephem sulfone. *Biochemistry* **2001**, *40*, 6233−6239.

(22) Trehan, I.; Beadle, B. M.; Shoichet, B. K. Inhibition of AmpC beta-lactamase through a destabilizing interaction in the active site. *Biochemistry* **2001**, *40*, 7992−7999.

(23) Lobkovsky, E.; Billings, E. M.; Moews, P. C.; Rahil, J.; Pratt, R. F.; et al. Crystallographic structure of a phosphonate derivative of the *Enterobacter cloacae* P99 cephalosporinase: mechanistic interpretation of a beta-lactamase transition-state analogue. *Biochemistry* **1994**, *33*, 6762−6772.

(24) Caselli, E.; Powers, R. A.; Blaszczak, L. C.; Wu, C. Y.; Prati, F.; et al. Energetic, structural, and antimicrobial analyses of beta-lactam side chain recognition by beta-lactamases. *Chem. Biol.* **2001**, *8*, 17−31.

(25) Powers, R. A.; Blazquez, J.; Weston, G. S.; Morosini, M. I.; Baquero, F.; et al. The complexed structure and antimicrobial activity of a nonbeta-lactam inhibitor of AmpC beta-lactamase. *Protein Sci.* **1999**, *8*, 2330−2337.

(26) Tondi, D.; Powers, R. A.; Caselli, E.; Negri, M. C.; Blazquez, J.; et al. Structure-based design and in-parallel synthesis of inhibitors of AmpC beta-lactamase. *Chem. Biol.* **2001**, *8*, 593−611.

(27) Cartwright, S. J.; Waley, S. G. Purification of beta-lactamases by affinity chromatography on phenylboronic acid-agarose. *Biochem. J.* **1984**, *221*, 505−512.

(28) Laskowski, R. A.; MacArthur, M. W.; Moss, D. S.; Thornton, J. M. PROCHECK: a program to check the stereochemical quality of protein structures. *J. Appl. Crystallogr.* **1993**, *26*, 283−291.

(29) Xu, Y.; Soto, G.; Hirsch, K. R.; Pratt, R. F. Kinetics and mechanism of the hydrolysis of depsipeptides catalyzed by the beta-lactamase of Enterobacter cloacae P99. *Biochemistry* **1996**, *35*, 3595−3603.

(30) Strynadka, N. C.; Adachi, H.; Jensen, S. E.; Johns, K.; Sielecki, A.; et al. Molecular structure of the acyl-enzyme intermediate in beta-lactam hydrolysis at 1.7 A resolution. *Nature* **1992**, *359*, 700−705.

(31) Kuzin, A. P.; Liu, H.; Kelly, J. A.; Knox, J. R. Binding of cephalothin and cefotaxime to D-ala-D-ala-peptidase reveals a functional basis of a natural mutation in a low-affinity penicillin-binding protein and in extended-spectrum beta-lactamases. *Biochemistry* **1995**, *34*, 9532−9540.

(32) Chen, C. C.; Herzberg, O. Structures of the acyl-enzyme complexes of the Staphylococcus aureus beta-lactamase mutant Glu166Asp: Asn170Gln with benzylpenicillin and cephaloridine. *Biochemistry* **2001**, *40*, 2351−2358.

(33) Powers, R. A.; Caselli, E.; Focia, P. J.; Prati, F.; Shoichet, B. K. Structures of ceftazidime and its transition-state analogue in complex with AmpC beta-lactamase: Implications for resistance mutations and inhibitor design. *Biochemistry* **2001**, *40*, 9207−9214.

(34) Lee, W.; McDonough, M. A.; Kotra, L.; Li, Z. H.; Silvaggi, N. R.; et al. A 1.2-A snapshot of the final step of bacterial cell wall biosynthesis. *Proc. Natl. Acad. Sci. U.S.A.* **2001**, *98*, 1427−1431.

(35) Murphy, B. P.; Pratt, R. F. Evidence for an oxyanion hole in serine beta-lactamases and DD- peptidases. *Biochem. J.* **1988**, *256*, 669−672.

(36) Chen, C. C.; Herzberg, O. Inhibition of beta-lactamase by clavulanate. Trapped intermediates in cryocrystallographic studies. *J. Mol. Biol.* **1992**, *224*, 1103−1113.

(37) Kelly, J. A.; Kuzin, A. P. The refined crystallographic structure of a DD-peptidase penicillin- target enzyme at 1.6 A resolution. *J. Mol. Biol.* **1995**, *254*, 223−236.

(38) Swaren, P.; Maveyraud, L.; Raquet, X.; Cabantous, S.; Duez, C.; et al. X-ray analysis of the NMC-A beta-lactamase at 1.64-A resolution, a class A carbapenemase with broad substrate specificity. *J. Biol. Chem.* **1998**, *273*, 26714−26721.

(39) Gordon, E.; Mouz, N.; Duee, E.; Dideberg, O. The crystal structure of the penicillin-binding protein 2x from *Streptococcus pneumoniae* and its acyl-enzyme form: implication in drug resistance. *J. Mol. Biol.* **2000**, *299*, 477−485.

(40) Maveyraud, L.; Golemi, D.; Kotra, L. P.; Tranier, S.; Vakulenko, S.; et al. Insights into class D beta-lactamases are revealed by the crystal structure of the OXA10 enzyme from *Pseudomonas aeruginosa*. *Structure* **2000**, *8*, 1289−1298.

(41) Paetzel, M.; Danel, F.; de Castro, L.; Mosimann, S. C.; Page, M. G.; et al. Crystal structure of the class D beta-lactamase OXA-10. *Nat. Struct. Biol.* **2000**, *7*, 918−925.

(42) Waley, S. G. A quick method for the determination of inhibition constants. *Biochem. J.* **1982**, *205*, 631−633.

(43) Weston, G. S.; Blazquez, J.; Baquero, F.; Shoichet, B. K. Structure-based enhancement of boronic acid-based inhibitors of AmpC beta-lactamase. *J. Med. Chem.* **1998**, *41*, 4577−4586.

(44) Varetto, L.; De Meester, F.; Monnaie, D.; Marchand-Brynaert, J.; Dive, G.; et al. The importance of the negative charge of beta-lactam compounds in the interactions with active-site serine DD-peptidases and beta-lactamases. *Biochem. J.* **1991**, *278*, 801−807.

(45) Strynadka, N. C.; Martin, R.; Jensen, S. E.; Gold, M.; Jones, J. B. Structure-based design of a potent transition state analogue for TEM-1 beta-lactamase. *Nat. Struct. Biol.* **1996**, *3*, 688−695.

(46) Luzzati, P. V. Traitment statistique des erreurs dans la determination des structure cristallines. *Acta Crystallogr.* **1952**, *5*, 802−810.

(47) Ness, S.; Martin, R.; Kindler, A. M.; Paetzel, M.; Gold, M.; et al. Structure-based design guides the improved efficacy of deacylation transition state analogue inhibitors of TEM-1 beta-lactamase. *Biochemistry* **2000**, *39*, 5312−5321.

(48) Kumar, S.; Pearson, A. L.; Pratt, R. F. Design, synthesis, and evaluation of alpha-ketoheterocycles as class C beta-lactamase inhibitors. *Bioorg. Med. Chem.* **2001**, *9*, 2035−2044.

(49) Otwinowski, Z.; Minor, W. Processing of X-ray diffraction data collected in oscillation mode. *Methods Enzymol.* **1997**, *276*, 307−326.

(50) Brunger, A. T. *X-PLOR Version 3.1 A system for X-ray crystallography and NMR*; Yale University Press: New Haven, CT, 1992; p 382.

(51) Brunger, A. T.; Adams, P. D.; Clore, G. M.; DeLano, W. L.; Gros, P.; et al. Crystallography & NMR system: A new software suite for macromolecular structure determination. *Acta Crystallogr., Sect. D* **1998**, *54*, 905−921.

(52) Jones, T. A.; Zou, J. Y.; Cowan, S. W.; Kjeldgaard, M. Improved methods for building protein models in electron-density maps and the location of errors in these models. *Acta Crystallogr., Sect. A* **1991**, *47*, 110−119.

(53) Kleywegt, G. J. Experimental assessment of differences between related protein crystal structures. *Acta Crystallogr., Sect. D* **1999**, *55*, 1878−1884.

(54) Kleywegt, G. J.; Jones, T. A. Software for handling macromolecular envelopes. *Acta Crystallogr., Sect. D* **1999**, *55*, 941−944.

(55) Brooks, B. R.; Bruccoleri, R. E.; Olafson, B. D.; States, D. J.; Swaminathan, S.; et al. Charmm − a Program for Macromolecular Energy, Minimization, and Dynamics Calculations. *J. Comput. Chem.* **1983**, *4*, 187−217.

(56) Laskowski, R. A. SURFNET: a program for visualizing molecular surfaces, cavities, and intermolecular interactions. *J. Mol. Graph.* **1995**, *13*, 323−330, 307−308.

(57) Zhang, X. J.; Matthews, B. W. EDPDB − a multifunctional tool for protein-structure analysis. *J. Appl. Crystallogr.* **1995**, *28*, 624−630.

(58) Connolly, M. L. Analytical molecular surface calculation. *J. Appl. Crystallogr.* **1983**, *16*, 548−558.

(59) Ferrin, T. E.; Huang, C. C.; Jarvis, L. E.; Langridge, R. The MIDAS display system. *J. Mol. Graph.* **1988**, *6*, 13−27.

(60) Evans, S. V. SETOR: hardware-lighted three-dimensional solid model representations of macromolecules. *J. Mol. Graph.* **1993**, *11*, 134−138.